Check for updates

Journal of Water & Health

IWA PUBLISHING

© 2022 The Authors

Journal of Water and Health Vol 20 No 11, 1629 doi: 10.2166/wh.2022.069

Role of a novel cationic gemini surfactant (CGS) on a one-step sol–gel process and photocatalytic properties of TiO_2 powders

Melek Koç Keşir [a,*], İkbal Sarıkaya Yıldız[a], Selçuk Bilgen[a] and Münevver Sökmen[b]

[a] Department of Chemistry, Karadeniz Technical University, Trabzon 61080, Turkey
[b] Department of Bioengineering, Konya Food and Agriculture University, Konya 42080, Turkey
*Corresponding author. E-mail: kocmelek612013@gmail.com

MK, 0000-0001-8905-2664

ABSTRACT

TiO_2 nanoparticles were prepared using a sol–gel process in combination with a novel cationic gemini surfactant (CGS) with amide functional groups at low temperatures. Titanium (IV) isopropoxide (TIP) and CGS were used as the starting materials and as effective agents, respectively, to orient the nanoparticles during the sol–gel synthesis. To reveal both the structural and morphological properties of the nanopowders prepared in this work, they were characterized using X-ray diffraction (XRD) analysis, scanning electron microscope (SEM), and Brunauer–Emmett–Teller (BET) surface area apparatus. The pore volume and pore size were calculated using the Barrett–Joyner–Halenda (BJH) model on the desorption branch. The experimental results show that the surface area and average crystallite size of the obtained TiO_2 nanopowders vary between 160–203 m^2/g and 27–49 nm, respectively. It was observed that the N_2 adsorption–desorption isotherms for almost all samples of TiO_2–*X*% CGS (*X*: mass of CGS) show the typical Type I with a hysteresis loop of H4. The photocatalytic activities of the CGS-modified nanocomposites are evaluated not only by the photocatalytic degradation of methyl orange (MO) but also by the reduction of Cr(VI) as model pollutants in the presence of visible light.

Key words: cationic gemini surfactant, Cr(VI), methyl orange (MO), photocatalysis, sol–gel, TiO_2

HIGHLIGHTS

- Excitable TiO_2/CGS composites were prepared by the sol-gel method.
- XRD, SEM, BET, and N_2 adsorption-desorption measurements were done for structural properties.
- Photocatalytic activity of TiO_2/CGS nanocomposite was evaluated on both the photoreduction of Cr(VI) ions and photooxidation of methyl orange under irradiation from a 365 nm lamp.
- Utilized in this survey is a cationic gemini surfactant that has a similar CTAB structure and has two long chains and cationic head groups and is a preferred morphology agents. Compared to one head group with CTAB, a novel synthesized cationic surfactant with two long chains is anticipated to positively affect both the properties of catalyst structures and data of photocatalytic degradation of model pollutants.

1. INTRODUCTION

Titanium dioxide (TiO_2) is used for the remediation of polluted aquatic systems because of its excellent photocatalytic properties. Pollutant derivatives do not transfer from aqueous to another phase during photocatalysis performed based on TiO_2 and do not cause the secondary pollution trouble contrary to conventional methods such as adsorption, biological methods, chlorination, ozonation, and their combinations widely used for treating the dye/Cr(VI)-containing wastewaters. Ultimately, it is also used in innovative techniques, including less time-consuming, more effective, and inexpensive methods. However, there are some general problems for the effective use of TiO_2. First, TiO_2 can only be applied with UV irradiation due to the wide bandgap being ~3.2 eV; thereby, no visible light response is obtained. Second, a high recombination rate of photogenerated charge carriers occurred on the surface of TiO_2 semiconductor, decreasing the photocatalytic efficiency. Third, the separation of the TiO_2 nanoparticles from water. To overcome these problems, many technical approaches such as modification with metal ions, and non-metals, coupling with other semiconductor, dye sensitization, and support materials such

This is an Open Access article distributed under the terms of the Creative Commons Attribution Licence (CC BY 4.0), which permits copying, adaptation and redistribution, provided the original work is properly cited (http://creativecommons.org/licenses/by/4.0/).

Downloaded from http://iwaponline.com/jwh/article-pdf/20/11/1629/1139570/jwh0201629.pdf
by guest

as glass slides, metal or ceramic substrates, polymer films, optical fibers have been developed to improve the photocatalytic activity (Altın *et al.* 2016b; Hoang *et al.* 2021). The surface area of the photocatalyst is another crucial factor in photocatalytic operations. A large surface area and high photoactivity are the desired properties of an effective photocatalyst. However, in the sol–gel technique, it is very troublesome to control both these properties and the agglomeration of TiO_2 nanoparticles because of the high surface energy of the nanometer materials.

Recently, surfactants have been used to eliminate these drawbacks of the photocatalyst and improve the catalytic performance. Their molecular structures and amphiphilic properties determine their orientation and formation of micelles on the surface at the stage of early preparation in the synthesis of the nanopowders, and thus can be used as stabilizers and dispersant agents. The dispersing effect of surfactants in the formation of TiO_2 particles provides a larger surface area and higher porosity. Sol–gel preparation of TiO_2 nanoparticles is the preferred method to obtain smaller particles and a large surface area. Surfactants provide a unique medium by keeping the nanoparticles apart from each other during nanoparticle formation. Therefore, the presence of a surfactant improves the photocatalytic efficiency of the catalyst by increasing the homogeneity of the sol–gel medium during nanoparticle formation.

Surfactants are known as amphiphilic molecules and are used in a wide range of industrial applications (Akbaş *et al.* 2012; Mohd Noh *et al.* 2017). Due to their great potential, they are used in many fields (Negm *et al.* 2013; Rosen *et al.* 2015; Nwidee *et al.* 2017; Sarıkaya *et al.* 2021). The application of surfactants and the surfactant-mediated production of nanoparticles have attracted great interest (Nogueira *et al.* 2015; Xu *et al.* 2015). Nanoparticle fabrication requires different strategies to bulk material fabrication and should be conducted (Khamhaengpol & Siri 2016; Shaban *et al.* 2019). It has been detected that SDBS (sodium dodecyl benzene sulfonate), CTAB, and TX-100 used to control the morphologies and structures of TiO_2/reduced grapheme oxide (TiO_2/RGO) as anionic, cationic, and non-ionic surfactants enhanced the catalyst surface area from 153 to 277 m^2/g. The enhanced surface area of the (TiO_2/RGO) samples contributed a considerable extent to the photocatalytic degradation of methylene blue due to not only high surface area but also to its inhibiting the reunion of the (e^-/h^+) pairs that occurred on the catalyst surface in the presence of irradiation (Hu *et al.* 2017). Choi *et al.* (2006) used the surfactant polyethylene glycol sorbitan monooleate to prepare TiO_2 nanoparticles and thin films. It was reported that the material has better structural and catalytic properties due to the anatase crystal phase, in addition to the high surface area, large pore volume and controlled pore size. The crystallite size is reported to be smaller with high crystallinity. A thermally stable spherical porous structure has been reported to exhibit four times higher photocatalytic activity, possibly due to a highly interconnected network in the crystal structure. Sodium dodecyl sulphate (SDS) surfactant was used as a capping agent to tailor the morphology of the $K_2V_3O_8$ by Basu *et al.* (2022). It was reported that the nanocomposites prepared by adding 0.2 g SDS reflected the highest BET surface area (23.6 m^2/g) compared to pure $K_2V_3O_8$ and 0.1-SDS/$K_2V_3O_8$. Moreover, it was determined that the average of $K_2V_3O_8$ samples decreased by 75 and 50 nm for particle size 0.1-SDS/$K_2V_3O_8$ and 0.2-SDS/ $K_2V_3O_8$, respectively. CTAB, SDS, and PVP-modified TiO_2 particles were evaluated in photocatalytic degradation of MB. TiO_2 with surfactants photocatalytically indicated degradation efficiency due to the properties of the surface in an hour and less time (Alphas Jebasingh *et al.* 2020). Another study was conducted by Anderson and Russell using the Tween surfactant to prepare TiO_2 thin films (Anderson & Russell 2014). Sol–gel TiO_2 production was modified by the addition of the non-ionic surfactant Triton X-100 (Stathatos *et al.* 2004; Altın *et al.* 2016a). It can be easily removed from the reaction medium. Similarly, the TiO_2 catalyst was prepared by the sol–gel method using polyethyleneimine or Pluronic P-123 as the surfactant (Galkina *et al.* 2011). Structural differences of the cationic surfactants, e.g., chain lengths, counterions, etc., provide different properties for the sol–gel preparation of TiO_2. Cetyl-trimethylammonium bromide (CTAB), cetyl-trimethylammonium chloride (CTAC), benzalkonium chloride (BC), and octadecyl-trimethyl ammonium bromide (C_{18}TAB) were employed by Casino *et al.* (2014) and the obtained nanoparticles demonstrated the desired porous properties and enhanced large specific surface area. MgO/g-C_3N_4 nanocomposite generated by the surfactant-assisted hydrothermal method was analyzed in both degradations of aqueous Malachite Green solution (25 ppm) and assessment of antimicrobial activity against the Gram-positive and Gram-negative bacteria. They explained that increasing specific surface area of MgO/g-C_3N_4 nanocomposite enhanced the number of active sites for absorption, improving the contact with the dye pigments, which in turn causes enhancement of photocatalytic performance (Madona & Sridevi 2022). In another study, nano-sized TiO_2 particles were prepared using a microwave-assisted sol–gel reaction. Jang *et al.* (2016) used polyvinylpyrrolidone (PVP, Mw: ~55,000), Triton X-100 (laboratory grade) and poly (ethylene glycol) triblock copolymer (P123, Mn: 5,800) to prepare TiO_2 spheres with sizes ranging from 105 to 380 nm. It has been reported that Triton X-100 and P123 have higher performance in the photocatalytic removal of methylene blue. Triton TX-100 is the most common surfactant and yields TiO_2 nanoparticles of very good quality (Altın *et al.* 2016a; Jang

Downloaded from http://iwaponline.com/jwh/article-pdf/20/11/1629/1139570/jwh0201629.pdf
by guest

et al. 2016). It is a non-ionic surfactant containing a hydrophilic polyethylene oxide chain and a hydrophobic p-(2, 4, 4-trimethylpentan-3-yl) phenyl ether group. Modification of the surfactant structure can be a good alternative for photocatalytic applications. First, the novel dicationic surfactants with functional groups rich in nitrogen atoms that provide increased electronic charge density and length of hydrophobic tail create the TiO_2 particles' resistance to aggregation in time. On the other hand, increasing the number of head groups in surfactant structure leads to electrostatic interaction with the prepared TiO_2 and steric barriers to protect the nanoparticles from aggregation (Shaban *et al.* 2019). Thus, monodispersed TiO_2 nano materials can produce high homogenous surface area with more active sites in the wastewater treatment. Not only the type of surfactant but also the conditions of sol–gel synthesis, such as pH, are important for the preparation of TiO_2 (Loosli & Stoll 2017; Tsega & Dejene 2017).

The F–N co-doped TiO_2 photocatalyst was prepared using CTAB, a cationic surfactant, and showed six times higher photoactivity than pure TiO_2. It was reported that the intensity of XRD peaks increased with increasing CTAB concentration and crystallization (Xie *et al.* 2008). Tashiro & Yamazaki (2019) constructed ZnTPyP fibers by the surfactant-assisted method exploring CTAB and kinetic study on the degradation of Rhodamine B (RhB). In another study, CTAB was used as an agent to control the catalyst surface, which exhibited different properties depending on the amount of surfactant and directly affected the photocatalytic activity (Wang *et al.* 2020). It is also known that CTAB as a cationic surfactant can form a cationic $C_{19}H_{42}N^+$ group, which is hydrophobic and can affect the growth of nanoparticles through electrostatic and steric effects. It has been noted that the $ZnWO_4$ nanomaterials fabricated a simple co-precipitation method using three different surfactants (PVP, SDS, and HMTA) and exhibited successful photocatalytic activity to degrade ciprofloxacin (CIP) antibiotic due to hampering the coagulation (Sivaganesh *et al.* 2020). In another study, surfactants were used to synthesize the nano-micro AgCl crystals in the growth of AgCl crystals (Zhou *et al.* 2022). In addition, the morphology of the manufactured products may have a specific structure because the CTAB molecules restrict the agglomeration of the particles. Our material, a cationic gemini surfactant (CGS) ($C_{40}H_{84}O_2N_4Br_2$), which is similar to the CTAB structure used in this study, has two long chains and cationic head groups, and is preferred as a morphology agent. It was proved that the critical micelle concentration (CMC) of CGS, whose physicochemical properties at different temperatures were determined in the previous literature, is lower than the concentration of CTAB (Sarıkaya *et al.* 2019). Due to the fact that CGS with much lower CMC values has higher surface activity, CGS was selected as a surfactant. It could be intriguing to investigate how the double chain structure together with the cationic head groups affects the structure of the catalyst in sol–gel synthesis and what contribution this CGS could make to the photocatalytic activity. As shown in Figure 8, the surface of TiO_2 nanoparticles is positively charged at inherent pH (pH < 6.8), since the zero point of charge (pzc) of TiO_2 (Degussa P25) is at pH 6.8, while it is negatively charged under alkaline conditions (pH > 6.8). As indicated, $C_{40}H_{84}O_2N_4Br_2$ is a cationic surfactant with a positive charge throughout and TiO_2 is adsorbed on the surface of gemini surfactant, which exerts a strong electrostatic repulsive force between them, which helps to hinder the aggregation of nanoparticles and enhance the more homogeneous surface.

In this study, TiO_2 nanoparticles were prepared by the sol–gel process in combination with a novel CGS with amide functional groups. *N, N′*-bis [3-(dodecanoylamino) propyl]-*N, N, N′, N′*-tetramethylhexane-1, 6-diammonium dibromide is the full chemical name, and the structure of the molecule is given below in Figure 1.

This CGS has been prepared previously and its preparation and chemical properties have been described in detail (Sarıkaya *et al.* 2019). Due to their amphiphilic nature, they form micelles at a certain concentration, which is called the CMC. The CMC value of CGS was determined by conductivity measurements of pure surfactant solutions, and is 7.41×10^{-4} M at 303.15 K. The structure may be an advantage for the preparation of TiO_2 nanoparticles. As can be seen from the molecular structure of CGS, it is a dicationic surfactant and can be an effective agent for nanoparticle alignment. TiO_2 nanoparticles were prepared as both naked TiO_2 and TiO_2–CGS during the sol–gel process. This is the first study in which CGS was

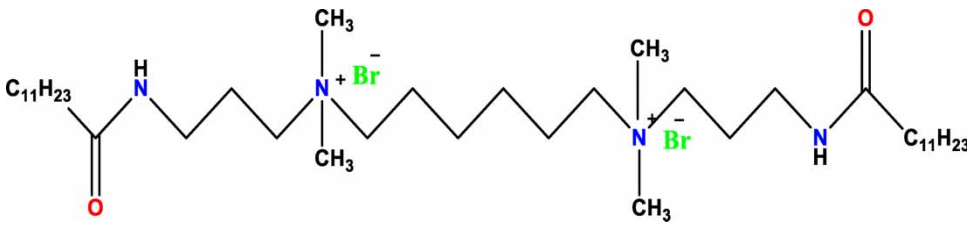


Figure 1 | *N, N′*-bis [3-(dodecanoylamino) propyl]-*N, N, N′, N′*-tetramethylhexane-1,6-diammonium dibromide (Sarıkaya *et al.* 2019).

Downloaded from http://iwaponline.com/jwh/article-pdf/20/11/1629/1139570/jwh0201629.pdf
by guest

used as a surfactant. The calcination temperature was kept low (300 °C) to maintain the organic carbon and nitrogen after the formation of the nanoparticles. This is particularly important to obtain a nanoparticle surface attractive for strong absorption of organic molecules. The crystal structure and optical properties of the nanoparticles were investigated by the SEM, BET, XRD, and UV-Vis DRS methods. The photocatalytic properties of the characterized nanoparticles were tested for aqueous Cr(VI) or methyl orange (MO) (10 mg/L) as inorganic and organic model pollutants under visible light exposure. If their discharges to the aquatic environment from the metallurgical industry and leather industry are above the limit values, they will be malefic for all living species (Liu *et al.* 2022; Zhang *et al.* 2022). High concentrations of hexavalent chromium ion Cr(VI) in systems can heavily damage the immune system of aquatic animals and induce human respiratory nervous system, cardiovascular and cerebrovascular diseases because of the rich mobility of Cr(VI). Thus, the effective way is the reduction of Cr(VI) to Cr(III), which have poor mobility and low toxicity. On the other hand, the highly soluble synthetic MO that comprises azo groups such as auxochrome and chromophore discharges to underground or aboveground from textile, paint, plastic, and cosmetic with rapid industrialization, and consequently, wastewater containing MO dye may be carcinogenic and mutagenic if discharged without treatment and negatively affect all live species (Al-Mamun *et al.* 2022). So, TiO_2 based on photocatalysis is one of the impressive solutions for degradation, mineralization of organic dyes, and reduction of inorganic materials.

2. MATERIALS AND METHODS

2.1. Synthesis of CGS

In the first step, 3-(dimethylamino)-1-propylamine (0.1 mol) was weighed into a round-bottom flask and dissolved in chloroform under an inert atmosphere. Dodecanoyl chloride (0.1 mol) was slowly added dropwise while stirring. The chloroform layers were extracted with saturated potassium carbonate solution, water, and brine, respectively. It was then dried with anhydrous calcium chloride. Finally, the chloroform was removed under a reduced pressure. In the second step, N-[3-(dimethylamino)propyl]dodecanamide (0.08 mol) and 1,6-dibromohexane (0.04 mol) were mixed in a flask and the mixture was refluxed in acetone through stirring at 60 °C for 6 h under nitrogen atmosphere. This product was washed and purified three times by recrystallization in cold acetone. The CGS was obtained as a white powder (Sarıkaya *et al.* 2019).

2.2. Preparation of TiO_2–CGS photocatalysts by the sol–gel method

Titanium (IV) isopropoxide (TIP) was used as a precursor, and all solvents and additional chemicals were of analytical grade. The details of the method are given in Figure 2 (Altın *et al.* 2016a).

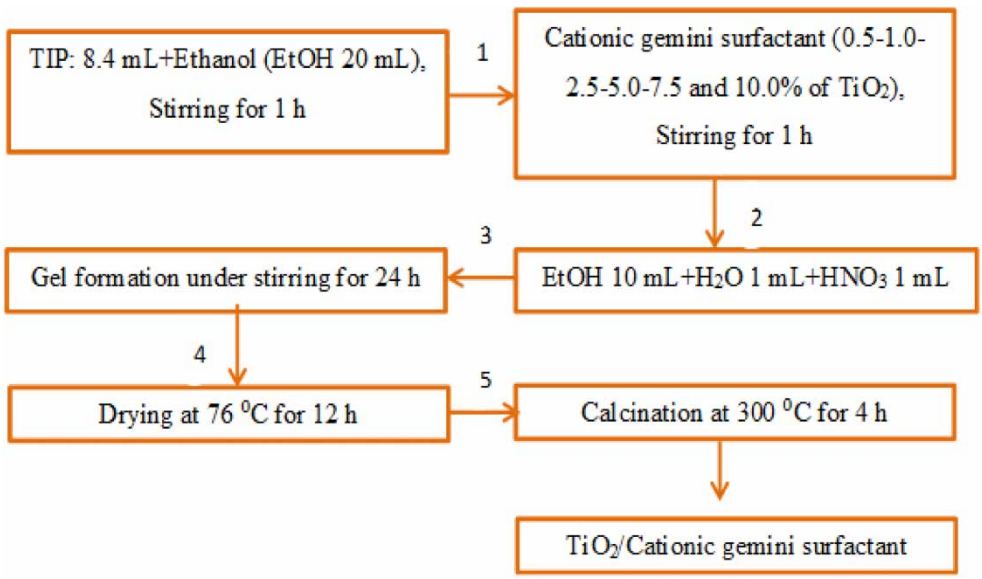


Figure 2 | Preparation process of TiO_2–CGS via the sol–gel method.

Downloaded from http://iwaponline.com/jwh/article-pdf/20/11/1629/1139570/jwh0201629.pdf
by guest

First, TIP (8.4 mL) was dissolved in 20 mL of absolute ethanol. The CGS was added to the solution at different percentages (10.71; 21.56; 53.90; 107.80; 161.70 and 215.6 mg CGS, corresponding to 0.5; 1.0; 2.5; 5.0; 7.5 and 10% of TiO_2 mass, respectively) and keft stirred (1 h). On the other hand, 1 mL of concentrated HNO_3 and 1 mL of distilled water were added to 10 mL of absolute ethanol and this mixture was added dropwise (extremely slow) to the first solution with vigorous mixing.

The mixture was stirred overnight and at the end of stirring, the mixture was dried at 76 °C for 12 h. The dried solid powder was calcined at 300 °C for 4 h. After cooling to room temperature, it was kept in dark bottles until use. TiO_2 powder was also prepared by the same procedure without surfactant. The hydrolysis step was quite slow, especially under vigorous stirring. We have reported the sol–gel method and the calcination temperature applied to prepare the desired photoactive TiO_2 nanoparticle (Altın *et al.* 2016a).

2.3. Characterization of TiO_2–CGS photocatalysts

Structural characterization of the produced nanoparticles was performed. XRD analysis of the catalysts was carried out using a Rigaku Smartlab diffractometer with CuKα radiation ($\lambda = 1.5406$ A°) over the range $2\theta = 20°$–$60°$ at room temperature. The surface morphology of the photocatalysts was studied using an SEM (JEOL, JSM 6610). The surface area, pore volume, pore size and crystallite size were determined by BET analysis (Oantachrome Autosorb IQ2).

2.4. Photocatalytic tests

Details of the photocatalytic assays have been described in previous work (Koç Keşir *et al.* 2020). A portion of 10 mg/L of Cr(VI) solution (250 mL) was placed in a quartz photoreactor and the pH was adjusted to 2.0 with H_3PO_4. This was preferred because the pH at the zero point of charge (pH_{pzc}) of the TiO_2 is 6.0–7.5, and the TiO_2 surface is positively charged at a lower pH. The surface absorption of the anionic Cr(VI) ions on the catalyst allow better contact between the surface and the Cr(VI) ions. The studied concentration of Cr(VI) solution was quite high compared to the values found in the real environment. The produced photocatalyst (1.0 g/L) was added to the test solution with magnetic stirring. The suspension was illuminated with a 365-nm lamp (6 W, Spectroline ENF-260; the light intensity of 350 $\mu W/cm^2$) for a specified exposure time. Every 30 min, a 2.0-mL sample of the suspension was taken to determine the remaining Cr(VI) ion concentration. The sample was centrifuged for 5 min to separate the solid catalyst (3,000 rpm, Eppendorf Centrifuge 5180) and filtered (0.45 μm membrane). The supernatant was used for further measurements. The photocatalytic tests were repeated with TiO_2 nanoparticles prepared by the same sol–gel procedure without surfactant. All experiments were repeated in the presence and absence of light (light and dark experiments). The remaining Cr(VI) ions were determined by the standard method EPA (7196A) (Environmental Protection Agency) after staining with diphenylcarbazide. Percent removal was calculated using the remaining Cr(VI) ion concentration after treatment. The same procedure was performed for the degradation of MO at $pH = 6$ (the natural pH of the aqueous solution of MO). The photocatalytic efficiency of the catalysts was measured by spectrophotometric monitoring of the absorbance of MO at 464 nm (Unicam UV-2 spectrometer) in the presence and absence (darkness) of light. A 250-mL portion of the aqueous solution of MO (10 mg/L) and 0.25 g of catalyst (1 g/L) were added to the photoreactor. The same sampling and separation steps were applied. The initial concentration of MO was also higher than the actual values found in the wastewater stream. These high concentrations were used specifically to prove that the catalyst was effective under severe conditions. Removal rates were calculated using the remaining MO concentration after treatment. Each test (for removal of MO or Cr(VI) ions) was repeated three times and the relative standard deviations were generally less than 1%.

3. RESULTS AND DISCUSSION

3.1. Structural analysis

As is well known, the nanocrystalline structure of TiO_2 is controlled by the method of preparation and subsequent calcination (Loosli & Stoll 2017; Tsega & Dejene 2017). The presence of a surfactant and its concentration can affect the fine structure of the catalyst. Calcination at low temperature such as 300 °C is sufficient to obtain the most active anatase crystal structure (Koç Keşir *et al.* 2020) because it has been found that as the temperature increases, the probability of rutile content increases as well as the anatase phase (Stathatos *et al.* 2004). Therefore, this temperature is suitable to keep the remaining carbon and nitrogen as well as the organic-mediated surface of the catalyst.

The typical XRD patterns of the anatase TiO_2 are shown in Figure 3. The XRD pattern of TiO_2 and their derivatives were in agreement with the JCPDS Card no. 21-1272, presenting the characteristic diffraction peaks (approximately centered at 2θ: 25.4°, 38°, 48° and 54.4°) that belong to the (1 0 1), (2 0 0), (0 0 4) and (1 0 5) planes of the anatase structure of synthesized

Downloaded from http://iwaponline.com/jwh/article-pdf/20/11/1629/1139570/jwh0201629.pdf
by guest

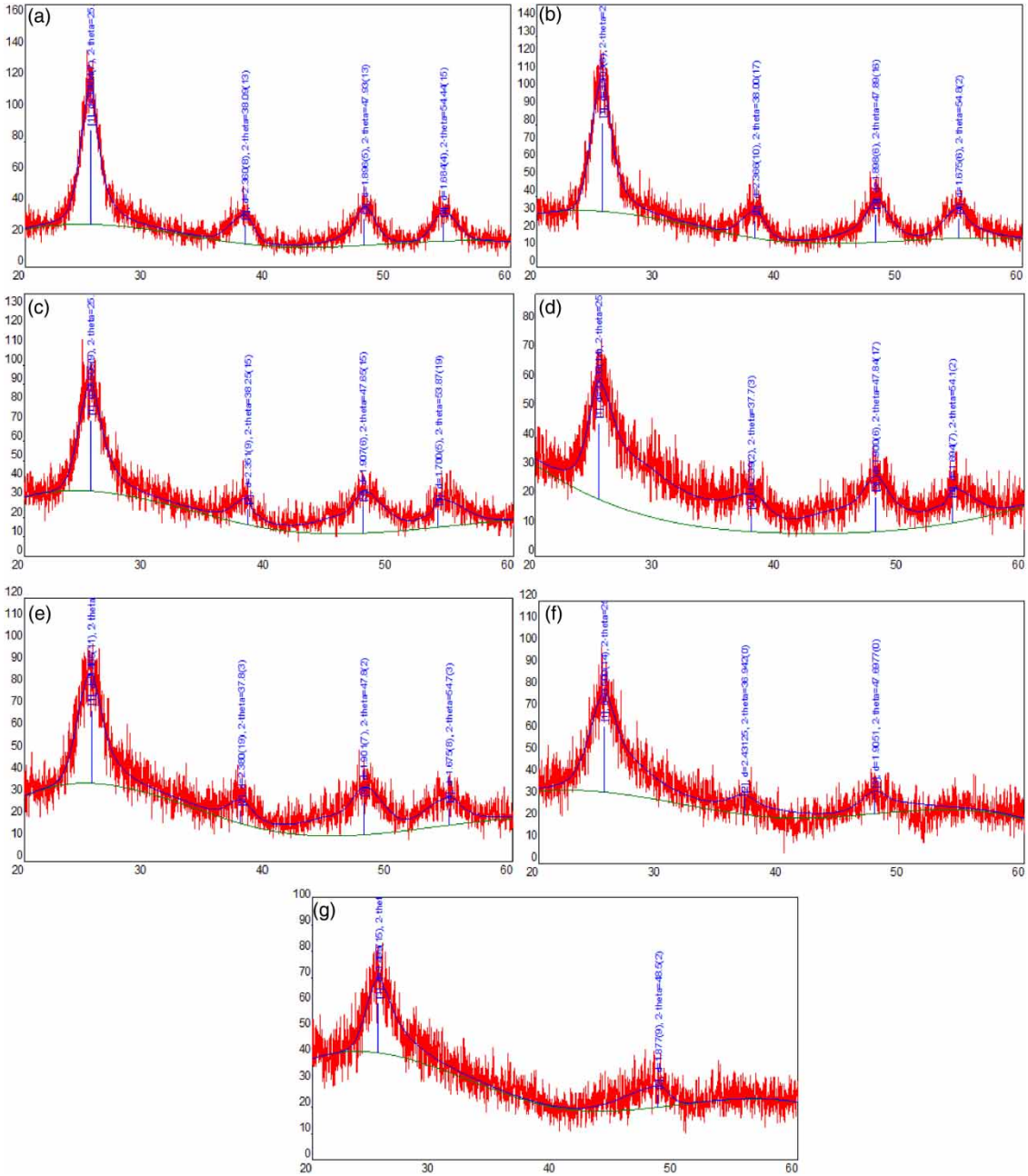


Figure 3 | XRD patterns of (a) TiO_2, (b) TiO_2–0.5%CGS, (c) TiO_2–1%CGS, (d) TiO_2–2.5%CGS, (e) TiO_2–5%CGS, (f) TiO_2–7.5%CGS and (g) TiO_2–10% CGS.

nanoparticles. No impurity was observed. The peak positions of nanoparticles did not have any changes in the presence of CGS. The XRD data indicated that the CGS loaded onto the surface of TiO_2 had no effect on the crystal structure of TiO_2 nanoparticles, which means that anatase TiO_2 is obtained when it is calcined at this temperature. This is because the melting point of CGS is 196.0–197.0 °C, so CGS probably decays when calcined at 300 °C. The crystalline structure has changed from anatase to amorphous by increasing the surfactant (e–f). It should be kept in mind that all catalysts were calcined at low temperature (300 °C). If the calcination temperature had been higher than 300 °C, the anatase form would have been obtained. It is known that photocatalytic activity is correlated with the crystallinity of photocatalysts. Thus, the following average crystallite sizes: TiO_2 TiO_2–0.5%CGS; TiO_2–1%CGS; TiO_2–2.5%CGS; TiO_2–5%CGS; TiO_2–7.5%CGS; TiO_2–10% CGS by using the Scherrer formula based on the (101) peak were evaluated. The average crystallite sizes of TiO_2–CGS

Downloaded from http://iwaponline.com/jwh/article-pdf/20/11/1629/1139570/jwh0201629.pdf
by guest

samples were calculated to be 49.4, 43.4, 37.5, 26.6, 36.2, 27.5, and 31.5 nm for TiO_2 and TiO_2–CGS (0.5–1.0–2.5–5.0–7.5–10%, resp.), which indicated that crystallite sizes of TiO_2 nanoparticles were decreased in the presence of CGS up to a certain concentration of CGS. It is conceivable that CGS used in TiO_2 nanoparticles synthesis via the sol–gel process did not change the peak positions of the anatase structure, but CGS molecules have a particular effect on the crystallite size of TiO_2 particles.

The images of SEM are given in Figure 4. The structural properties were similar, and no significant differences were observed. This could be because the organic template either could not be removed during heat treatment or covered the active pores of the TiO_2 surface or broke the pore structure (Choi *et al.* 2007). It could also be because either the realignment of the particles within the sample results in poor dispersibility and aggregation of the particles when the template is used, or it does not help the particles to move away from each other (Wu *et al.* 2018). However, the analyses of BET revealed more supportive structural properties.

N_2 adsorption–desorption measurement at a temperature of 77.4 K for liquid N_2 was also used to measure structural properties. The nitrogen sorption–desorption isotherm curves are shown in Figure 5.

The isotherms for almost all samples of TiO_2–X% CGS (X: mass of CGS) exhibited typical type I with an H4 type hysteresis loop (defined by IUPAC) expressing slit pores, including pores in the micropore region. Type I isotherms are that adsorption is be restricted to the depletion of a single monolayer (Langmuir adsorption) of pollutants on the photocatalyst surface. Type H4 hysteresis is also often associated with narrow slit pores. The hysteresis loop in the relative pressure (P/P_0) region of 0.1–0.99 may be due to the fact that once filled with adsorbate, the pores leave little or no external surface for further adsorption. Incorporating CGS to the microporous TiO_2 lattice in the synthesis step does not collapse the TiO_2 micropores structure and thus does not alter the isotherms' behaviors. Figure 5(b) shows that the BJH pore size distribution curves obtained from the N_2 adsorption–desorption measurements of the different samples are too narrow and the majority

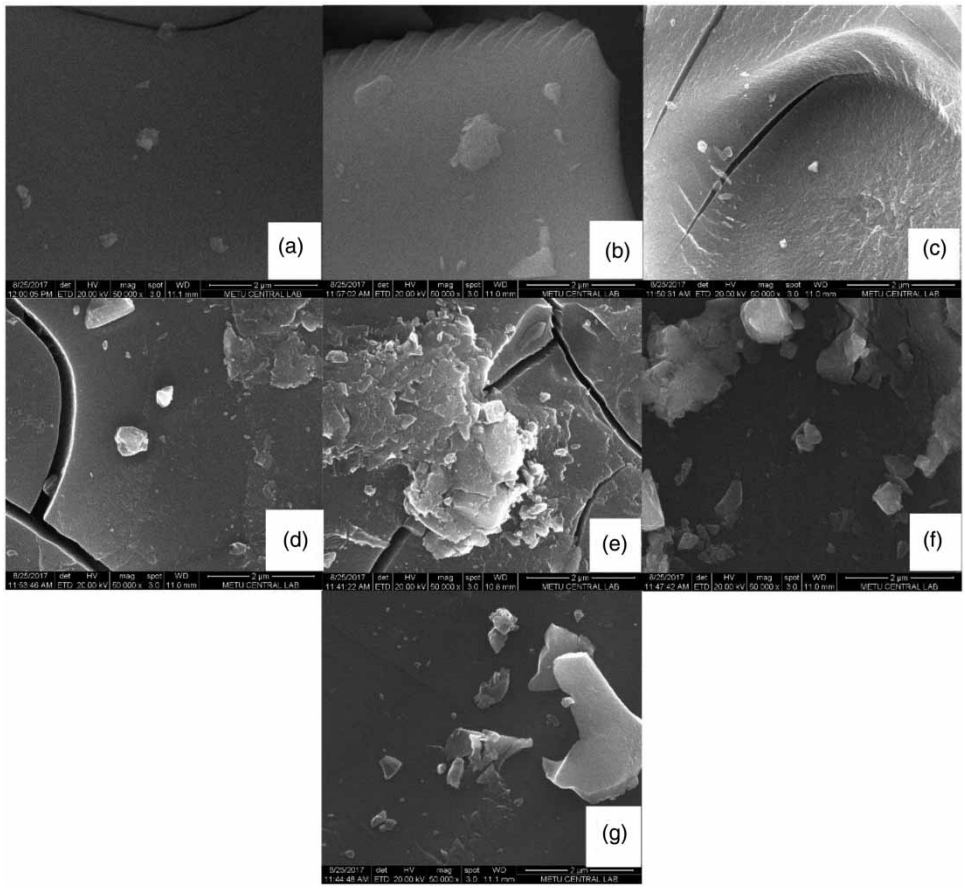


Figure 4 | SEM images of the TiO_2 catalysts at a 2-μm scale. (a) TiO_2, (b) TiO_2–0.5% CGS, (c) TiO_2–1%CGS, (d) TiO_2–2.5%CGS, (e) TiO_2–5%CGS, (f) TiO_2–7.5%CGS and (g) TiO_2–10%CGS.

Downloaded from http://iwaponline.com/jwh/article-pdf/20/11/1629/1139570/jwh0201629.pdf
by guest

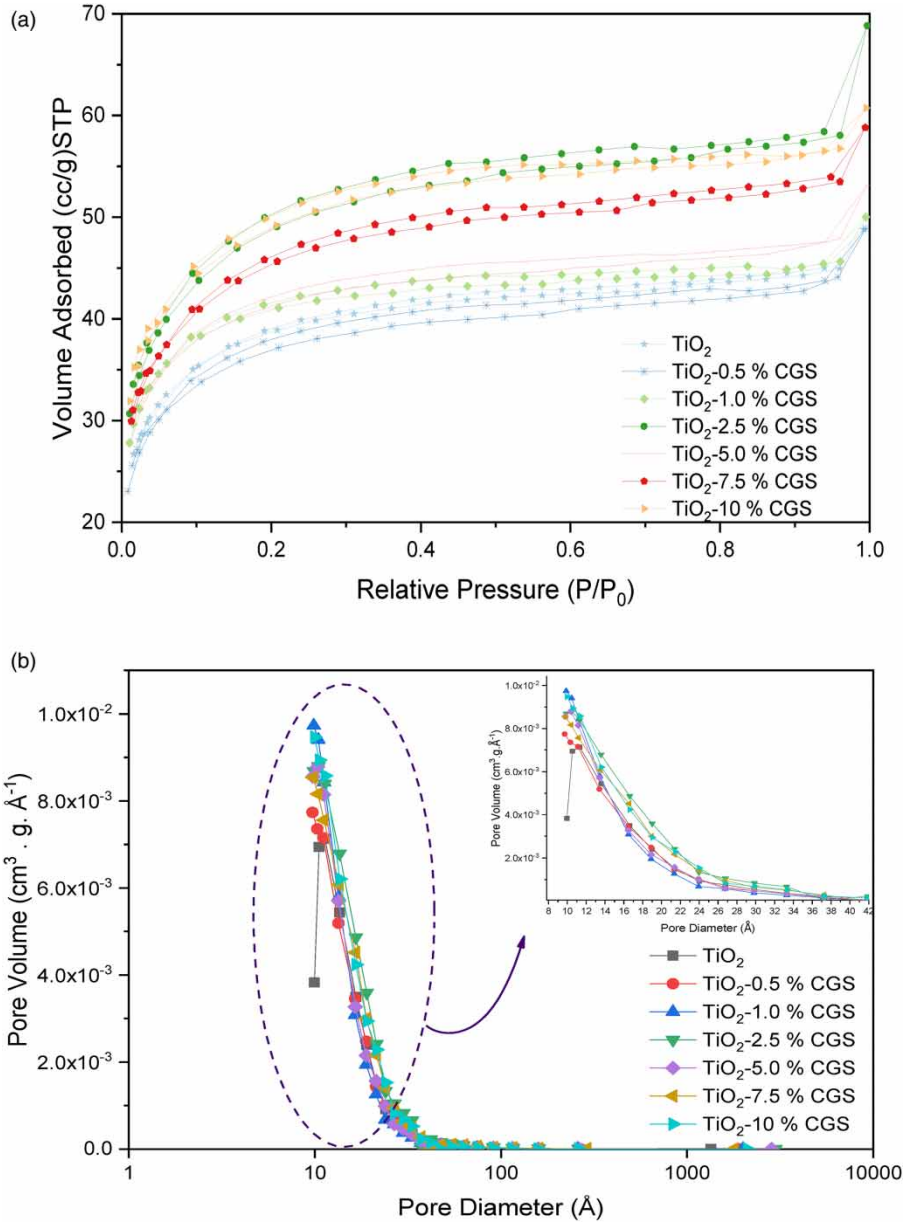


Figure 5 | (a) Nitrogen sorption–desorption isotherms and (b) pore size distribution curves of pure and TiO_2–0.5–10%CGS.

aperture is centered at about 10 Å. This indicates that all TiO_2 including CGS molecules have a microporous structure. CGS may be partially covered the surface of TiO_2 and blocked its pore channels. Also, as the mass ratio of CGS increase to 2.5% CGS, BET surface area and pore volumes of TiO_2–*X*% CGS nanoparticles enhance regularly. Yet, when surfactant used more than 2.5% CGS, the rise in both surface area and pore volume values is greater than naked TiO_2 sample and smaller than mass ratio of 0.5–2.5% CGS. The increase in the surface area corresponds to crystallite size, thus validating that adding CGS improves the TiO_2 surface properties to prevent particle aggregation, resulting in the decrease of crystallite size. The low surface area and pore volume may affect photocatalytic efficiency depending on structural, morphological incides and nature of pollutants. Detailed values of BET such as surface area, total pore volume, and pore size parameters are shown in Table 1.

As seen from Table 1, the prepared TiO_2 has quite a large surface area with or without CGS. The surface area and pore size of both pure TiO_2 particles and TiO_2–X% CGS are in the range of 160–220 m^2/g and 9.7–11.3 Å, respectively.

Downloaded from http://iwaponline.com/jwh/article-pdf/20/11/1629/1139570/jwh0201629.pdf
by guest

Table 1 | BET analyses of prepared TiO_2 catalysts

	Surface area[a]	Pore volume[b]	Pore size[c]	Crystallite size[d]
(a)	160.0	0.0703	11.320	49.3
(b)	203.3	0.0859	9.973	43.4
(c)	220.0	0.1047	10.47	37.5
(d)	201.3	0.0883	9.795	26.6
(e)	180.8	0.0768	10.36	36.2
(f)	177.5	0.0714	9.871	27.5
(g)	170.2	0.0742	9.708	31.5

Note: (a) TiO_2, (b) TiO_2–0.5%CGS, (c) TiO_2–1%CGS, (d) TiO_2–2.5%CGS, (e) TiO_2–5%CGS, (f) TiO_2–7.5%CGS, (g) TiO_2–10%CGS.
[a]Multipoint BET, BJH method cumulative desorption surface area (m^2/g).
[b]The BJH method cumulative desorption pore volume (cc/g).
[c]The BJH method desorption pore diameter (mode) (Å).
[d]Calculated by the Scherrer equation (nm).

The surface area of pure TiO_2 was 160.0 m^2/g, and it was increased to 160.0–220.0 m^2/g in the presence of CGS. These values are almost 10 times higher than those of TiO_2 produced in the presence of surfactant Triton-TX100. It should be noted that very slow hydrolysis and vigorous mixing are applied during the sol–gel process. This could have an important impact on the production of small but porous particles with a large surface area. The cumulative desorption surface area increases by increasing the CGS concentration used during the sol–gel process. While TiO_2 prepared without surfactant had a surface area of 160.0 m^2/g, it increased up to 220 m^2/g and then remained almost stable. The highest surface area was obtained when 1.0% CGS was used in the sol–gel process. Other parameters such as pore volume, pore size and crystallite size exhibited the same trend. Pore volume increased, pore size and crystallite size decreased with increasing CGS concentration. This result directly confirms that the CGS micelles play a major role in the increasing of surface area, which enhances the synergistic effect between adsorption and photocatalysis with the help of dicationic CGS molecules. Thus, more active adsorption and photocatalytic reaction can be provided by an enlarged surface area of synthesized TiO_2 samples with CGS. Moreover, repulsive forces such as electrostatic and steric can be formed on the surface of TiO_2 nanoparticles because of dispersing CGS with double cationic head groups. This means that dispersibility of the nanoparticles in synthesis solution was enhanced and the aggregation rate of particles was reduced. The contribution of CGS to the physical and chemical structure of TiO_2 enables control of both the crystallite size and surface features of nanoparticles.

3.2. Photocatalytic removal of Cr(VI) and MO

All TiO_2 catalysts were tested separately for photoreduction for Cr(VI) ions and photooxidation for MO. Prior to light exposure, the catalysts were tested for the removal of the target pollutants in the dark. The percentages of removal of Cr(VI) ions and MO are shown in Figures 6 and 7, respectively.

The removal process depends on the surface area and crystallite size of the catalyst. As the surface area increases and the crystallite size decreases, the number of active sites responsible for photocatalytic degradation increases. Therefore, more Cr(VI) and MO molecules are adsorbed and the degradation increases. Both degradation data of Cr(VI) were in good agreement with the results of BET surface area and particle size. As seen in Table 1, the maximum specific surface area and crystallite size were found to be 220 m^2/g and 27 nm for TiO_2–1.0% CGS nanoparticles. Furthermore, in the photocatalytic reduction of Cr(VI) with TiO_2–1.0% CGS nanoparticles, it was calculated that the reduction efficiency was 77.22% at an initial concentration of 10 mg/L of Cr(VI) after 150-min irradiation (Figure 6). The capacity of the catalyst to remove Cr(VI) was higher than that of pure TiO_2 (33.42%) and TiO_2 prepared in the presence of TX-100 (40%) under the same experimental conditions (Altın *et al.* 2016a). CGS played a significant role in increasing the dispersion of titanium dioxide particles in the sol–gel reaction media, and CGS surfactant at a ratio of 1.0% greatly increased the removal efficiency of Cr(VI). This could be due to the sufficient mass of surfactant molecules, which increased the morphological and structural properties to enhance Cr(VI) removal. It appeared that the Cr(VI) removal efficiency was decreased steadily with increasing CGS content. The decrease in removal efficiency was due to the aggregation of CGS on the TiO_2 surface after the TiO_2 surface reached saturation with respect to the surfactant. In contrast to the photocatalytic reduction of Cr(VI), MO was quite resistant to

Downloaded from http://iwaponline.com/jwh/article-pdf/20/11/1629/1139570/jwh0201629.pdf
by guest

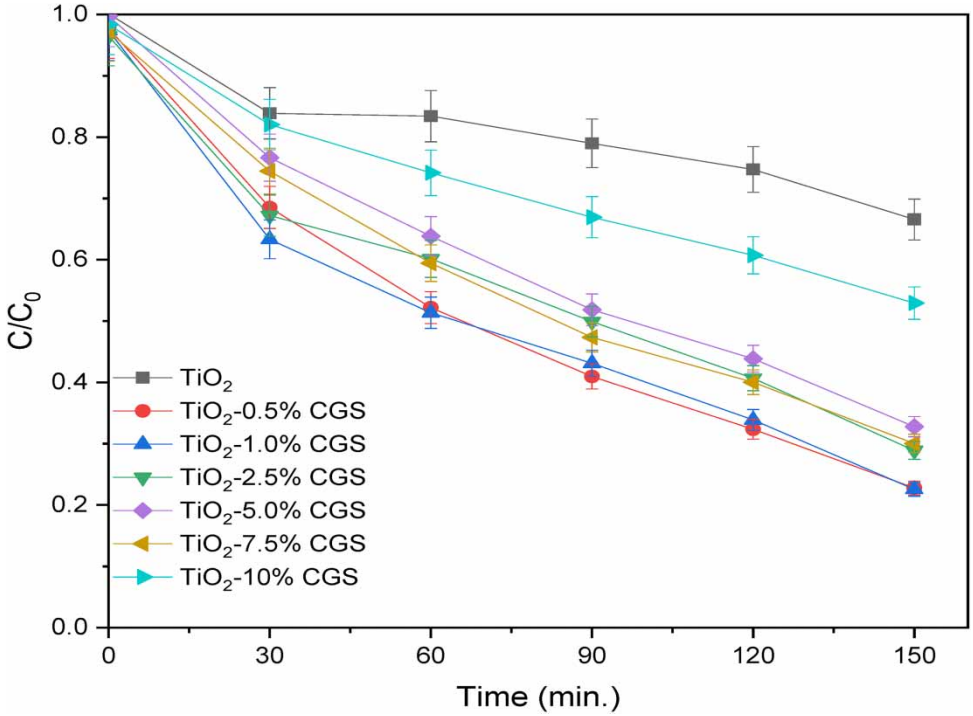


Figure 6 | The photocatalytic removal of Cr(VI) ions after visible light irradiation ($[C]_o = 10$ mg/L, catalyst mass = 1 g/L, pH = 2, $\lambda = 365$ nm).

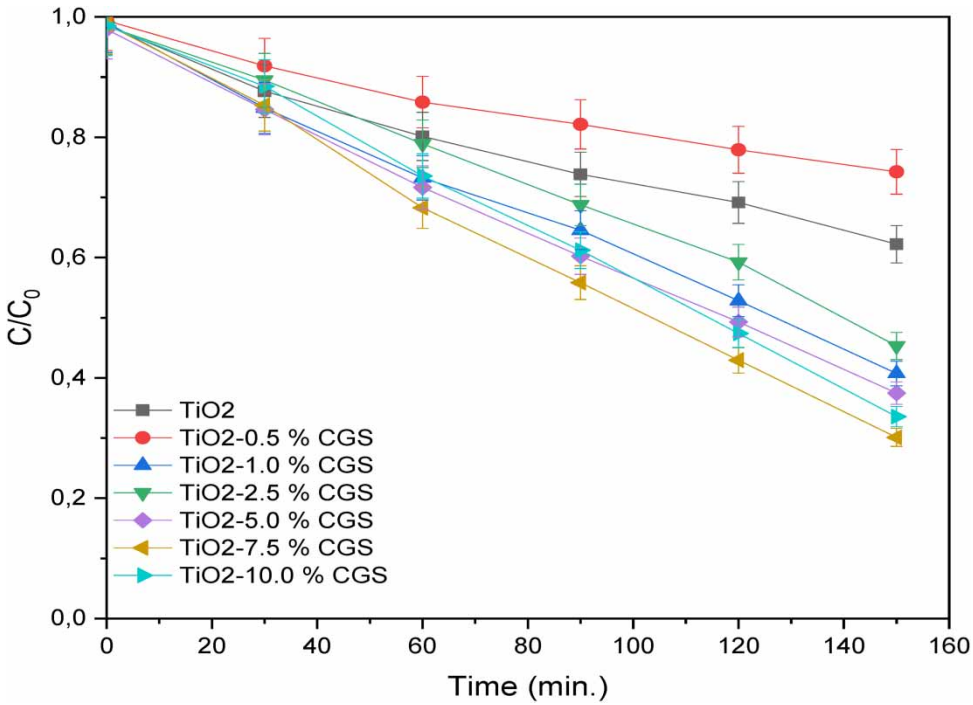


Figure 7 | The photocatalytic removal of MO after visible light irradiation ($[MO]_o = 10$ mg/L, catalyst mass = 1 g/L, pH = 6, $\lambda = 365$ nm).

photochemical degradation and the removal percentage was 59.27% with TiO_2–1.0% CGS for a 150-min irradiation period which is still higher than TiO_2 prepared in the presence of TX-100 (36.84%) (Altın *et al.* 2016a). The highest percentage of MO removal was obtained with TiO_2–7.5% CGS (69.89%) (Figure 7).

Downloaded from http://iwaponline.com/jwh/article-pdf/20/11/1629/1139570/jwh0201629.pdf
by guest

To calculate the apparent rate constant for the study of kinetic degradation of MO and Cr(VI), the loss of both pollutants was observed as a function of irradiation time, and the data were fitted to a first-order and zero-order rate model for Cr(VI) and MO, respectively, using the following equation:

The pseudo first-order equation is represented by

$$-\ln\left(\frac{C}{C_0}\right) = K_{app}\, t$$

Also, the zero-order equation is represented by

$$[C] = [C_0] - K_{app}t$$

where C_0 and C represent the concentrations of organic and inorganic pollutants at the initial stage (0 min) and after irradiation for some time (t: 150 min), and K_{app} is the pseudo first-order rate constant (min^{-1}) for photocatalytic degradation of pollutants. The kinetics parameters for the photocatalytic efficiency of the catalysts are presented in Table 2.

Logarithmic relationship of the ratio between the original concentration of pollutants (C) and the concentration after photocatalytic degradation (C_0) against the equaled irradiation time (min) yields a linear line. The slope of linear regression equals to the apparent first-order rate constant K_{app} (Riaz *et al.* 2020). The removal profiles of the Cr(VI) by the TiO_2–CGS derivatives fitted well to the pseudo first-order kinetics, the first-order kinetics defining chemical reaction is based on a hypothesis in which the reaction rate is linearly dependent on the concentration of only one reactant. In contrast, the MO degradation profile obeys zero-order kinetics, indicating that the catalytic sites (e^{-}/h^{+} pairs) on the surface of TiO_2–CGS can oxidize the MO molecules that diffuse to the surface of the photocatalyst in the irradiation time, and zero-order reactions are independent from reactant concentration.

As shown in Table 2, it was found that the rate constant (K_{app} value) of as-prepared TiO_2–7.5% CGS is 1.2 min^{-1} with the value of correlation coefficient (R^2: 0.98), exhibiting the fastest degradation rate for MO among the TiO_2 samples synthesized using CGS by a modified sol–gel method, which is greater than that of approximately 4.1, 2.5, 1.5, 1.3, 1.2 and 1.01 times belonging to TiO_2–0.5% CGS (0.29 min^{-1}), TiO_2 (0.48 min^{-1}), TiO_2–2.5% CGS (0.79 min^{-1}), TiO_2–1.0% CGS (0.89 min^{-1}), TiO_2–5.0% CGS (0.98 min^{-1}) and TiO_2–10% CGS (1.1 min^{-1}), respectively.

As for Cr(VI), the TiO_2–0.5% CGS and TiO_2–1.0% CGS samples were found to have a similar pseudo first-order rate constant of 1.48 (R^2: 0.99) and 1.49 min^{-1} (R^2: 0.97). However, among the produced nanoparticle samples, the TiO_2–1.0% CGS was preferred for comparing to first-order rate constant, because they have high removal percentage of Cr(VI) due to the biggest surface area and smallest crystallite size (Table 1). It was seen that the K_{app} values were in a descending sequence of 2.5% (1.24 min^{-1}) > 7.5% (1.2 min^{-1}) > 5.0% (1.1 min^{-1}) > 10% (0.64 min^{-1}) CGS > TiO_2 (0.41 min^{-1}) when the amount of CGS exceeded the 1.0%. The pseudo first-order rate constant of TiO_2–1.0% CGS particles is nearly higher than 3.66 (TiO_2), 2.40 (TiO_2–10% CGS), 1.34 (TiO_2–5.0% CGS), 1.24 (TiO_2–7.5% CGS) and 1.20 (TiO_2–2.5% CGS) times. These results could be ascribed to the blocking of active pores on the surface of the nanoparticles if there were undecayed surfactant

Table 2 | Kinetic parameters of pseudo first-order rate constants and zero-order of synthesized TiO_2 with various amounts of CGS after 150-min irradiation

	Pseudo first-order [Cr(VI)]		Zero-order (MO)	
Photocatalyst	**k_{app} (min^{-1})**	**R^2**	**k_{app} ($\frac{mol}{L}/min$)**	**R^2**
TiO_2	1.9×10^{-3}	0.89	1.7×10^{-3}	0.98
TiO_2–0.5% CGS	4.5×10^{-3}	0.99	1.2×10^{-3}	0.97
TiO_2–1.0% CGS	4.7×10^{-3}	0.97	2.8×10^{-3}	0.98
TiO_2–2.5% CGS	4.1×10^{-3}	0.96	2.6×10^{-3}	0.96
TiO_2–5.0% CGS	4.2×10^{-3}	0.99	2.9×10^{-3}	0.99
TiO_2–7.5% CGS	4.3×10^{-3}	0.99	3.4×10^{-3}	0.98
TiO_2–10% CGS	2.8×10^{-3}	0.97	3.2×10^{-3}	0.96

Downloaded from http://iwaponline.com/jwh/article-pdf/20/11/1629/1139570/jwh0201629.pdf
by guest

molecules in the calcination stage. This is because all the surfactants cannot be removed in the calcination stage, and the remaining CGS, which cannot be removed, may hamper the interaction of the excitation light with the active pores on the TiO_2 catalyst, causing a decrease in photoactivity, and may cause slower removal reaction. It can be surmised that the photo decolorization efficiency enhances with increasing K_{app} value. Almost all catalysts prepared with CGS were more effective than TiO_2 prepared without CGS in both dark and light conditions.

In the sol–gel production step (acid hydrolysis), the adsorption layer between CGS and TiO_2 nanoparticles can be formed by the electrostatic interactions (cationic CGS and positively charged TiO_2) as the TiO_2 particles are positively charged under the acid hydrolysis conditions and CGS is a dicationic surfactant. In this way, homogeneously dispersed TiO_2 nanomaterials can be obtained. This is because of the repulsive forces between the TiO_2 particles and CGS, which effectively prevents the agglomeration of particles. Therefore, surface interactions between TiO_2 and CGS are not expected to be much stronger than negatively charged surfactants. Thus, dicationic surfactant CGS can better generate repulsive forces than mono cationic surfactants. Moreover, CGS is a large molecule and provides a positively charged barrier between the TiO_2 nanoparticles formed right after extremely slow hydrolysis. The possible repulsive forces between TiO_2 particles and CGS molecules are schematically shown in Figure 8.

3.3. Clarification of photocatalytic mechanism of Cr(VI) and MO

The photocatalytic mechanism of MO degradation and Cr(VI) reduction may be stated as follows. When suspended TiO_2 nanoparticles in the aqueous Cr(VI) and MO solution were excited, photons with energy ($h\upsilon$) higher than or equal to the semiconductor bandgap (3.2 eV) cause electronic excitation for migration of electrons from valance band to conduction band (CB), and thus, electron and positive hole pairs (e^-/h^+) are generated, respectively, in the CB and valence band (VB) (1). These free electrons commonly scavenged by O_2 absorbed on the photocatalyst's surface produce superoxide radical anion ($O_2^{-\bullet}$) (3), which can pave the way for reactive oxygen species (ROS) (i.e., $^\bullet OH$, $O_2^{-\bullet}$, H_2O_2, $^1O_2$, etc.) It is universally acknowledged that the ROS are active radical species of catalytic processes. In addition, h^+ reacts with OH^- or H_2O to produce powerful unselective hydroxyl radicals ($^\bullet OH$) (2) as oxidants (with a redox potential of +2.80 V) (Kordouli *et al.* 2015).

$$TiO_2 + h\upsilon \rightarrow e_{CB}^- + h_{VB}^+ \quad (1)$$

$$h_{VB}^+ + H_2O \rightarrow HO^{\cdot} + H^+ \quad (2)$$

$$e_{CB}^- + O_2 \rightarrow O_2^{\cdot -} \quad (3)$$

$$Cr_2O_7 + 14H^+ + 6e_{CB}^- \rightarrow 2Cr^{3+} + 7H_2O \quad (4)$$

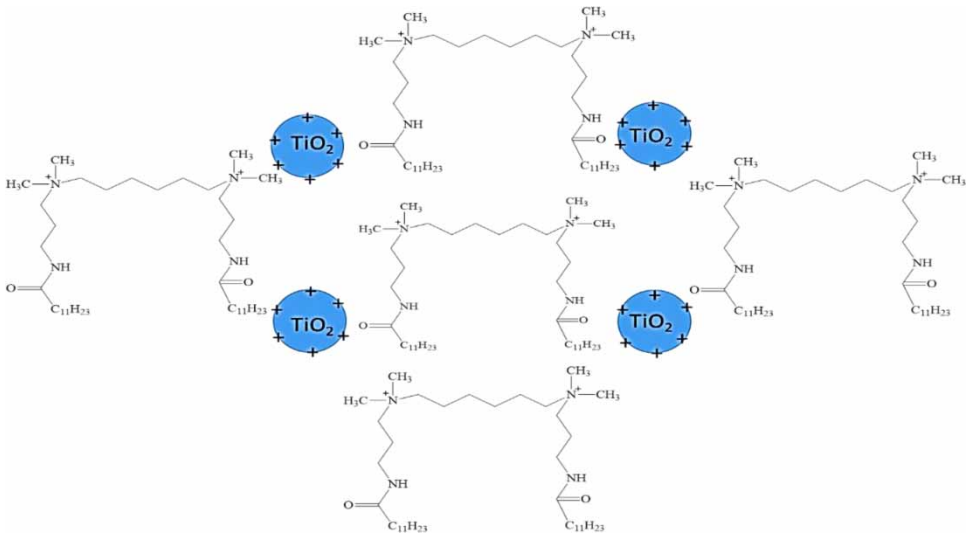


Figure 8 | Orientation of TiO_2 nanoparticles in the sol–gel medium.

Downloaded from http://iwaponline.com/jwh/article-pdf/20/11/1629/1139570/jwh0201629.pdf
by guest

$$H_2CrO_4 + 6H^+ + 3e^- \rightarrow Cr^{3+} + 4H_2O \quad (5)$$

$$HCrO_4^- + 7H^+ + 3e^- \rightarrow Cr^{3+} + 4H_2O \quad (6)$$

$$CrO_4^{2-} + 8H^+ + 3e_{CB}^- \rightarrow Cr^{3+} + 4H_2O \quad (7)$$

$$Cr\ (VI) + e_{cb}^- \rightarrow Cr\ (VI) + e_{CB}^- \rightarrow Cr\ (IV) + e_{CB}^- \rightarrow Cr\ (III) \quad (8)$$

$$HO^{\cdot} + MO \rightarrow by - product \rightarrow CO_2 + H_2O \quad (9)$$

While h^+, $^{\bullet}OH$ and $O_2^{-\bullet}$ subsequently decompose the dye molecules into mineral salts, CO_2 and H_2O as the end products (9) (Al-Mamun *et al.* 2022), electron (e^-) on the CB provides reduction to Cr(III) from Cr(VI) species in the pollutant solutions (4–8) (Djellabi *et al.* 2016).

4. CONCLUSION

In this work, a novel method for the preparation of TiO_2 nanoparticles by the sol–gel method employing a CGS with amide functional groups was described. The morphology of the catalyst was characterized by using XRD, SEM, and BET analyses, and the photocatalytic effect was evaluated using model pollutants. A surfactant with a double chain structure and cationic head groups was chosen for the sol–gel synthesis. The cationic CGS could not only improve the crystallinity but also enhance the morphological properties such as surface area, pore volume, pore size, and thus develop the photocatalytic performance. As a result of these findings, CGS could be recommended as a new surfactant for easy TiO_2 production. The amphiphilic nature and dicationic structure of this novel CGS with amide functional groups confer additional structural and surface properties to the well-known TiO_2. However, further mechanistic evaluation is needed.

DATA AVAILABILITY STATEMENT

All relevant data are included in the paper or its Supplementary Information.

CONFLICT OF INTEREST

The authors declare there is no conflict.

REFERENCES

Akbaş, H., Elemenli, A. & Boz, M. 2012 Aggregation and thermodynamic properties of some cationic gemini surfactants. *Journal of Surfactants and Detergents* **15** (1), 33–40.

Al-Mamun, M. R., Hossain, K. T., Mondal, S., Afroza Khatun, M., Islam, M. S. & Khan, M. Z. H. 2022 Synthesis, characterization, and photocatalytic performance of methyl orange in aqueous TiO_2 suspension under UV and solar light irradiation. *South African Journal of Chemical Engineering* **40**, 113–125.

Alphas Jebasingh, J., Stanley, R. & Vidyavathy, S. M. 2020 sol–gel preparation of surfactants assisted titania for solar photocatalysis. *Materials Letters* **279**, 128460.

Altın, İ., Sökmen, M. & Bıyıklıoğlu, Z. 2016a Quaternized zinc (II) phthalocyanine-sensitized TiO_2: surfactant-modified sol–gel synthesis, characterization and photocatalytic applications. *Desalination and Water Treatment* **57** (34), 16196–16207.

Altın, İ., Sökmen, M. & Bıyıklıoğlu, Z. 2016b Sol gel synthesis of cobalt doped TiO_2 and its dye sensitization for efficient pollutant removal. *Materials Science in Semiconductor Processing* **45**, 36–44.

Anderson, A. L. & Russell, B. 2014 The effect of tween® surfactants in sol–gel processing for the production of TiO_2 thin films. *Coating* **4** (4), 796–809.

Basu, S. S., Rahut, S., Bisht, A. S. & Basu, J. K. 2022 Surfactant-assisted tuning of $K_2V_3O_8$ nanorods for robust charge dynamics in semiconductor photocatalysis. *Materials Science in Semiconductor Processing* **147**, 106681.

Casino, S., Di Lupo, F., Francia, C., Tuel, A., Bodoardo, S. & Gerbaldi, C. 2014 Surfactant-assisted sol -gel preparation of high-surface area mesoporous TiO_2 nanocrystalline Li-ion battery anodes. *Journal of Alloys and Compounds* **594**, 114–121.

Choi, H., Stathatos, E. & Dionysiou, D. D. 2006 Synthesis of nanocrystalline photocatalytic TiO_2 thin films and particles using sol–gel method modified with nonionic surfactants. *Thin Solid Films* **510** (1–2), 107–114.

Choi, H., Stathatos, E. & Dionysiou, D. D. 2007 Effect of surfactant in a modified sol on the physicochemical properties and photocatalytic activity of crystalline TiO_2 nanoparticles. *Topics in Catalysis* **44**, 513–521.

Djellabi, R., Ghorab, F. M., Nouacer, S., Smara, A. & ve Khireddine, Q. 2016 Cr(VI) photocatalytic reduction under sun light followed by Cr(III) extraction from TiO_2 surface. *Materials Letters* **176**, 106–109.

Downloaded from http://iwaponline.com/jwh/article-pdf/20/11/1629/1139570/jwh0201629.pdf
by guest

Galkina, O. L., Vinogradov, V. V., Agafonov, A. V. & Vinogradov, A. V. 2011 Surfactant-assisted sol–gel synthesis of TiO_2 with uniform particle size distribution. *International Journal of Inorganic Chemistry* **2011**, 8. Article ID 108087.

Hu, J., Li, H., Muhammad, S., Wu, Q., Zhao, Y. & Jalio, Q. 2017 Surfactant-assisted hydrothermal synthesis of TiO_2/reduced graphene oxide nanocomposites and their photocatalytic performances. *Journal of Solid State Chemistry* **253**, 113–120.

Jang, I., Leong, H. J. & Oh, S. G. 2016 Effects of surfactants on the preparation of TiO_2 nanoparticles in microwave-assisted sol-gel process and their photocatalytic activity. *Korean Journal of Chemical Engineering* **33**, 1647–1652.

Khamhaengpol, A. & Siri, S. 2016 Fluorescent light mediated a green synthesis of silver nanoparticles using the protein extract of weaver ant larvae. *Journal of Photochemistry and Photobiology B: Biology* **163**, 337–344.

Koç Keşir, M., Dilber, G., Sökmen, M. & Durmuş, M. 2020 Use of new quaternized water soluble zinc phthalocyanin derivatives for effective dye sensitization of TiO_2. *Journal of Sol-Gel Science and Technology* **93**, 687–694.

Kordouli, E., Bourikas, K., Lycourghiotis, A. & Kordulis, C. 2015 The mechanism of azo-dyes adsorption on the titanium dioxide surface and their photocatalytic degradation over samples with various anatase/rutile ratios. *Catalysis Today* **252**, 128–135.

Liu, Y., Lin, Y., Tang, J., Liu, X., Chen, L., Tian, Y., Fang, D. & Wang, J. 2022 Preparation of a coated ZH-scheme (sns_2@CdS)/TiO_2(0 0 1) photocatalyst for phenol degradation with simultaneous Cr(VI) conversion. *Applied Surface Science* **574**, 151595.

Loosli, F. & Stoll, S. 2017 Effect of surfactants, pH and water hardness on the surface properties and agglomeration behavior of engineered TiO_2 nanoparticles. *Environmental Science: Nano Journal* **4**, 203–211.

Madona, J. & Sridevi, J. 2022 Surfactant assisted hydrothermal synthesis of MgO/g-C_3N_4 heterojunction nanocomposite for enhanced solar photocatalysis and antimicrobial activities. *Inorganic Chemistry Communications* **138**, 109265.

Mohd Noh, M. A., Khalid, K., Ariffin, A. & Khan, M. N. 2017 Counterion-induced cationic flexible nanoparticle catalytic of piperidinolysis of phenyl salicylate. *Journal of Surfactants and Detergents* **20**, 1075–1084.

Negm, N., El-Tabl, A. S., Aiad, I. A., Zakareya, K. & Moustafa, A. H. 2013 Synthesis, characterization, biodegradation and evaluation of the surface active properties of nonionic surfactants derived from jatropha oil. *Journal of Surfactants and Detergents* **16**, 857–863.

Nogueira, D. R., Scheeren, L. E., Vinardell, M. P., Mitjans, M., Infante, M. R. & Rolim, C. M. B. 2015 Nanoparticles incorporating pH-responsive surfactants as a viable approach to improve the intracellular drug delivery. *Materials Science and Engineering: C* **57**, 100–106.

Nwidee, L. N., Lebedev, M., Barifcani, A., Sarmadivaleh, M. & Iglauer, S. 2017 Wettability alteration of oil-wet limestone using surfactant-nanoparticle formulation. *Journal of Colloid and Interface Science* **504**, 334–345.

Riaz, N., Haasan, M., Siddique, M., Mahmood, Q., Farooq, U., Sarwar, R. & Saqib Khan, M. 2020 Photocatalytic degradation and kinetic modeling of azo dye using bimetallic photocatalysts: effect of synthesis and operational parameters. *Environmental Science and Pollution Research* **27**, 2992–3006.

Rosen, M. J., Wang, H., Shen, P. & Zhu, Y. 2015 Ultralow interfacial tension for enhanced oil recovery at very low surfactant concentrations. *Langmuir* **21**, 3749–3759.

Sarıkaya, İ., Bilgen, S. & Akbaş, S. 2019 Investigation of mixing behavior of both a conventional surfactant and different inorganic salts with a cationic gemini surfactant in aqueous solution. *Journal of Surfactants and Detergents* **22**, 1319–1330.

Sarıkaya, İ., Bilgen, S., Ünver, Y., Inan Bektaş, K. & Akbaş, H. 2021 Synthesis, characterization, antibacterial activity, and interfacial and micellar features of novel cationic gemini surfactants with different spacers. *Journal of Surfactants and Detergents* **24**, 909–921.

Shaban, S. M., Aiad, I., Yassin, F. A. & Mosalam, A. 2019 The tail effect of some prepared cationic surfactants on silver nanoparticle preparation and their surface, thermodynamic parameters, and antimicrobial activity. *Journal of Surfactants and Detergents* **22**, 1445–1460.

Sivaganesh, D., Saravanakumar, S., Sivakumar, V., Rajajeyaganthan, R., Arunpandian, M., Gopal, J. N. & Thirumalaisamy, T. K. 2020 Surfactants-assisted synthesis of ZnWO4 nanostructures: a view on photocatalysis, photoluminescence and electron density distribution analysis. *Materials Characterization* **159**, 110035.

Stathatos, E., Lianos, P. & Tsakiroglou, C. 2004 Highly efficient nanocrystalline titania films made from organic/inorganic nanocomposite gels. *Microporous and Mesoporous Materials* **75**, 255–260.

Tashiro, K. & Yamazaki, S. 2019 Photocatalysis of ZnTPyP fibers fabricated by surfactant-assisted method: effect of surfactant and kinetic studies. *Colloids and Surfaces A: Physicochemical and Engineering Aspects* **580**, 123741.

Tsega, M. & Dejene, F. B. 2017 Influence of acidic pH on the formulation of TiO_2 nanocrystalline powders with enhanced photoluminescence property. *Heliyon* **3**, e00246.

Tuyet Hoang, N. T., Kim Tran, A. T., An Le, T. & Duc Nguyen, D. 2021 Enhancing efficiency and photocatalytic activity of TiO_2-SiO_2 by combination of glycerol for MO degradation in continuous reactor under solar irradiation. *Journal of Environmental Chemical Engineering* **9** (5), 105789.

Wang, Y., Wang, Q., Zhang, H., Yue, W., Jia, Y., Jin, R. & Gao, S. 2020 CTAB-assisted solvothermal construction of hierarchical Bi_2MoO_6/Bi_5O_7Br with improved photocatalytic performances. *Separation and Purification Technology* **242**, 116775.

Wu, W., Zhang, L. & Zhai, X. 2018 Preparation and photocatalytic activity analysis of nanometer TiO_2 modified by surfactant. *Nanomaterials and Nanotechnology* **8**, 1.

Xie, Y., Zhao, X., Li, Y., Zhao, Q., Zhou, X. & Yuan, Q. 2008 CTAB-assisted synthesis of mesoporous F–N-codoped TiO_2 powders with high visible-light-driven catalytic activity and adsorption capacity. *Journal of Solid State Chemistry* **181**, 1936–1942.

Xu, L., Wang, Y., Wei, G., Feng, L., Dong, S. & Hao, J. 2015 Ordered DNA-surfactant hybrid nanospheres triggered by magnetic cationic surfactants for photon- and magneto-manipulated drug delivery and release. *Biomacromolecules* **16**, 4004–4012.

Downloaded from http://iwaponline.com/jwh/article-pdf/20/11/1629/1139570/jwh0201629.pdf
by guest

Zhang, H., Chen, L., Xu, B. & Ping, Y. 2022 Rhombic TiO_2 grown on g-C_3N_4 nanosheets towards fast charge transfer and enhanced Cr(VI) and NO removal. *Journal of Industrial and Engineering Chemistry* **111**, 226–234.

Zhou, M., Hu, X., Xu, X., Jing, Y., Lai, Y., Su, S., Mahmud, S., Zhang, X. & Zhu, J. 2022 Controlled synthesis of silver/silver chloride composite crystals from $[AgCl_2]^-$ complex and its photocatalysis properties on organic pollutants. *Colloids and Surfaces A: Physicochemical and Engineering Aspects* **647**, 128984.

First received 16 February 2022; accepted in revised form 15 October 2022. Available online 4 November 2022

Downloaded from http://iwaponline.com/jwh/article-pdf/20/11/1629/1139570/jwh0201629.pdf
by guest